Spectrochimica Acta Part A: Molecular and Biomolecular Spectroscopy 350 (2026) 127401

Contents lists available at ScienceDirect

Spectrochimica Acta Part A:
Molecular and Biomolecular Spectroscopy

journal homepage: www.journals.elsevier.com/spectrochimica-acta-part-a-molecular-and-biomolecular-spectroscopy

Human neuroglobin and H64A distal variant: How mutation and pH affect the heme pocket

Mirco Meglioli [a], Laura Cesati [b], Gianantonio Battistuzzi [a], Marco Borsari [a], Federico Sebastiani [b,c,d,*], Giulietta Smulevich [b,d,*]

[a] Department of Chemical and Geological Sciences, University of Modena and Reggio Emilia, via Campi 103, 41125 Modena, Italy
[b] Department of Chemistry "Ugo Schiff" DICUS, University of Florence, via della Lastruccia 3, 50019 Sesto Fiorentino (FI), Italy
[c] European Laboratory for Non-Linear Spectroscopy (LENS), Via Nello Carrara 1, 50019 Sesto Fiorentino (FI), Italy
[d] INSTM, Research Unit of Firenze, via della Lastruccia 3, 50019 Sesto Fiorentino (FI), Italy

HIGHLIGHTS

- At alkaline pH Lys67 protonation triggers the reorganization of the heme pocket.
- pH induces a rearrangement of the heme vinyls orientation.
- In distal His64Ala variant, pH induces the coordination of Lys67 to the heme iron.
- In His64Ala variant, pH induces readjustment of the propionate hydrogen-bonds.

GRAPHICAL ABSTRACT

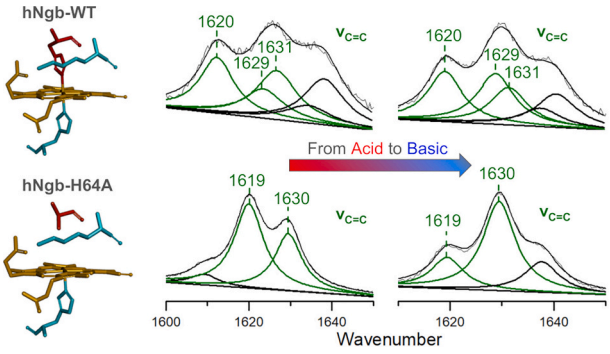

ARTICLE INFO

Keywords:
Resonance Raman spectroscopy
Magnetic circular dichroism
Vinyl and propionyl heme substituents
Heme rotational disorder

ABSTRACT

Neuroglobins (Ngbs) are low spin heme proteins, with His64 and His96 residues bound to the distal and proximal positions of the heme iron, respectively. His64 must be displaced to allow the ligation of exogenous molecules to the heme, thus regulating ligand binding. In fact, in the absence of the distal His, at physiological pH, the protein becomes high spin in both the ferric and ferrous states. However, the variant undergoes a pH-dependent coordination/spin state transition to a hexacoordinated low-spin species at alkaline pH, featuring Lys67 as the distal endogenous ligand. Here, we have investigated the effect of pH on the wild-type (WT) protein and the distal H64A variant of human Ngb in solution by a combination of UV–Vis electronic absorption, Magnetic Circular Dichroism and resonant Raman spectroscopies. In the WT protein, only a vinyl substituent conformational change is observed with increasing pH, due to the strong stability of the bis-histidyl heme coordination. Conversely, in the H64A variant alkaline pH induces a major structural rearrangement of the active site with the

Abbreviations: CD, Circular Dichroism; hNgb, human neuroglobin; hNgb-H64A and -H64V, human neuroglobin hNgb-His64Ala and -His64Val distal variants; Hb, hemoglobin; hNgb-H64AK67A, human neuroglobin hNgb-His64AlaLys67Ala distal variant; hNgb-C46AC55A, Cys46AlaCys55Ala human neuroglobin variant; Mb, myoglobin; MCD, Magnetic Circular Dichroism, RR: resonance Raman; 5c, 6c, penta- and hexacoordinated, HS, high spin; LS, low spin; WT, wild-type; p6 and p7, propionate group at positions 6 and 7, respectively; v2 and v4, vinyl group at positions 2 and 4, respectively.

* Corresponding authors at: Department of Chemistry "Ugo Schiff" DICUS, University of Florence, via della Lastruccia 3, 50019 Sesto Fiorentino (FI), Italy.
E-mail addresses: federico.sebastiani@unifi.it (F. Sebastiani), giulietta.smulevich@unifi.it (G. Smulevich).

https://doi.org/10.1016/j.saa.2025.127401
Received 6 October 2025; Received in revised form 4 December 2025; Accepted 27 December 2025
Available online 29 December 2025
1386-1425/© 2025 Elsevier B.V. All rights are reserved, including those for text and data mining, AI training, and similar technologies.

distal coordination of Lys67 to the heme, a change in the strength of the hydrogen bonds of the propionate groups and a conformational rearrangement of one vinyl substituent. We propose that these findings are due to the modifications in the *E*-helix as a consequence of Lys67 deprotonation in both the WT and the variant. These results provide further details at the molecular level on the fundamental role of distal residues for heme binding within the active site and protein stability.

1. Introduction

Neuroglobins (Ngbs) are hemeproteins expressed predominantly in neurons of the central and peripheral nervous system, but their low concentration in non-pathological brain tissues and high autoxidation rate hardly support an oxygen storage or carrier function [1,2]. Indeed, the functional role of Ngbs has been ascribed to the protection of neuronal tissues under hypoxic conditions as a consequence of an ischemic event, although the underlying molecular mechanism is still unclear [3,4]. These hemeproteins show the typical three-over-three α-helical globin fold, but unlike myoglobin (Mb) or hemoglobin (Hb), are hexacoordinated with His64(E7) and His96(F8) bound to the distal and proximal coordination positions of the heme Fe atom, respectively [5,6]. In addition to the bis-histidyl coordination, in the heme distal site of human and murine Ngbs, aromatic-electrostatic interactions with Phe28(B10) and Phe42(CD1), together with the apolar residue Val68 (E11), accommodate the porphyrin in the pocket, participating in the heme stabilization with Lys67(E10), whose nitrogen is H-bonded with the propionate substituents [7]. It has been, therefore, hypothesized that the presence of the large internal cavity (about 120 $Å^3$ in human Ngb), which is an extension of the heme crevice, might facilitate Ngb signaling activity by fast ligand-induced conformational changes [4]. However, many studies have demonstrated that especially the His64 residue is fundamental for regulating ligand binding, being its dissociation the rate-limiting step. The reactivity of hexacoordinated Ngb is then modulated by the strength of the His64-Fe bond rather than by the ligand accessibility to the heme pocket through the Lys67 gate, as reviewed in Ref. [8]. In fact, the distal Fe-ligand must be displaced to allow the binding of exogenous ligands like O_2, CO or NO to the ferrous heme, of sulfide to the ferric heme [4,9–12]. Several studies have been performed on the distal His64 variants of both murine and human neuroglobins [1,12–14]. In the absence of the distal His, the protein becomes high-spin, being hexa- and penta-coordinated in the ferric and ferrous states at physiological pH, respectively. However, it has been found that the variant undergoes a pH-dependent coordination/spin state transition to a hexacoordinated low-spin species, which dominates at alkaline pH, featuring Lys67 as the distal endogenous ligand [13–15].

Therefore, mutation of Ngb can enable to pinpoint key structural determinants in the heme pocket for regulating at the molecular level the function, still not completely clear, of neuroglobin. In particular, it is important to get insights into the role of His64 residue in the stabilization of the distal cavity and its interplay with Lys67 in heme ligation. For this purpose, in the present work, we have further investigated the effect of pH on the distal H64A variant human Ngb (hNgb) in comparison with the WT protein by UV–Vis electronic absorption, Magnetic Circular Dichroism (MCD), Circular Dichroism (CD) and resonant Raman (RR) spectroscopies.

2. Materials and methods

2.1. Protein expression and purification

Wild-type human neuroglobin (hNgb-WT, GenBank reference sequence AF422796) and the H64A variant (hNgb-H64A) were expressed in *E. coli*. The hNgb-WT expression system was already available [16], while the synthetic gene for (untagged) human Ngb-H64A variant was purchased from Integrated DNA Technologies (Coralville, IA, USA) and subcloned in the prokaryotic expression vector pLATE11 (aLICator Ligation Independent Cloning and Expression System; Thermo Scientific, Waltham, MA, USA). The vector was then inserted into a competent BL21 (DE3) *E. coli* strain containing the T7RNA polymerase gene controlled by IPTG-inducible lacUV5 promoter.

E. coli was grown at 37 °C in LB medium containing 100 μg/mL ampicillin. After reaching $OD_{600nm} = 0.6–0.8$, the culture was quenched to 25 °C and expression induced by adding 1 mL of a 2.5 mg/mL bovine hemin solution (10 mg in 4 mL of a 10 mM NaOH milliQ H_2O solution) and 1 mL of a 0.5 mM IPTG solution. Reddish cells were collected after 14–18 h by centrifugation at 5200 rpm × 10 min at 10 °C in 250 mL Nalgene™ tubes using a Beckman Coulter Allegra *V*-15R™ centrifuge, the supernatant was removed and pellet was stored at −20 °C until purification.

Protein purification started with cells resuspension in 50 mM Tris-HCl buffer pH 8.0 and disruption by sonication (1–1.5 h, 1 min of sonication +30 s of break, with centrifuge tube in an ice bath). To remove cells debris, two centrifugation steps in 50 mL tubes and one in 15 mL tubes at 11000 rpm × 20 min 20 °C were done using a Beckman Coulter Allegra *V*-15R™ centrifuge. Human Ngb-WT was precipitated in presence of 4 M $(NH_4)_2SO_4$ to further remove impurities and dialyzed in Tris-HCl 50 mM buffer at pH 8.0, whereas the H64A variant was not treated with ammonium sulphate precipitation to avoid NH_3 coordination to the heme iron. Both proteins were purified by weak anionic-exchange chromatography (Capto™ DEAE, Cytiva, using 50 mM Tris-HCl pH = 8.0 and 50 mM Tris-HCl + 200 mM NaCl pH 8.0 as binding and elution buffers, respectively) followed by size-exclusion chromatography (Superdex G-75, GE Healthcare Life Sciences) using 50 mM Tris-HCl + 150 mM NaCl pH = 7.0 as eluent buffer. The purified H64A variant was incubated for 1 h with a 10-fold excess of potassium ferricyanide to oxidize the heme iron [12] followed by a second SEC step to remove the $K_3[Fe(CN)_6]$ not reacted.

The purity of the proteins was checked by SDS gel electrophoresis (15 % acrylamide), which in both cases yielded a single band at around 17 kDa, corresponding to the calculated molecular mass of neuroglobin [14,17]. Both proteins were purified in aerobic conditions; therefore, they are characterized by the presence of a disulfide bridge between Cys46 and Cys55 [16,18,19].

2.2. Sample preparation

The proteins were diluted from stock solutions.

The samples of ferric hNgb-WT were prepared in 50 mM phosphate buffer with 0.1 M NaCl at pH 7.4 and titrated with HCl/NaOH in the pH range 3.7–12.3, while those containing ferric hNgb-H64A variant were prepared in 50 mM phosphate buffer with 0.1 M NaCl at pH 6 and 7.4, and in 50 mM Tris-HCl with 0.1 M NaCl at pH 10 and pH 12.

The ferrous species were obtained by reducing the ferric proteins with few μL of freshly prepared sodium dithionite solutions (20 mg/mL for WT protein and 10 mg/mL for H64A variant in 50 mM phosphate buffer with 0.1 M NaCl at pH 7.4), after extensive degassing with N_2 gas (Rivoira, Milano, Italy). The ferrous hNgb-WT was prepared in 50 mM phosphate buffer with 0.1 M NaCl at pH 5.2 and 7.4, and in 100 mM phosphate buffer with 0.1 M NaCl at pH 11.4, while the ferrous hNgb-H64A variant was prepared in 50 mM phosphate buffer with 0.1 M NaCl at pH 6 and 7.4, and in 50 mM Tris-HCl with 0.1 M NaCl at pH 9.

Protein concentration was about 40 μM for both the ferric and ferrous samples.

2.3. Electronic absorption measurements

The electronic absorption measurements were performed with a Cary60 spectrophotometer (Agilent, Santa Clara, CA, USA) with a resolution of 1.5 nm and a 300 nm/min scan rate at room temperature. The samples were placed either in a 1 mm cuvette or a 5 mm NMR tube, and measured before and after each resonant Raman measurement to assess that no degradation of the samples occurred under the experimental conditions used. The second derivative spectra were obtained by applying the Savitzky-Golay method on 15 data points with a third-order polynomial (LabCalc; Galactic Industries, Salem, NH). No significant difference in the wavelength or in the bandwidth were observed when the number of points was changed. All the spectra were normalized to the maximum intensity of the Soret band, and the intensity in the visible region was further magnified for clear visualization, as indicated in the captions of the figures.

2.4. Magnetic Circular Dichroism and Circular Dichroism

Magnetic Circular Dichroism (MCD) and Circular Dichroism (CD) measurements were performed at 25 °C using a Jasco J-810 spectropolarimeter (JASCO Corporation, Tokyo, Japan) using quartz cuvettes of 0.5 and 1 cm path length, respectively. MCD spectra were recorded at 200 nm/min scan rate with a resolution of 1.0 nm, summing up 12 spectra in the Soret region and 8 spectra in the Q bands region to improve the signal-to-noise ratio. All experiments were carried out with protein solutions freshly prepared before use, around 8 μM and 60 μM in the Soret and Q bands regions respectively, in 50 mM phosphate buffer plus 100 mM NaCl at pH 7.0 and titrated with HCl/NaOH. The magnetic field for MCD measurements was provided by a Model 3470 GMW Magnet split coil superconductivity magnet (Redwood City, CA, USA) with a maximum field of 1 T. MCD spectra were measured in θ = mdeg and converted to $\Delta\varepsilon$ [$M^{-1}\cdot cm^{-1}\cdot T^{-1}$] using the conversion factor $\Delta\varepsilon = \theta/(32{,}980\cdot c\cdot d\cdot B)$, where c is the protein concentration, d is the thickness of the sample (path length = 0.5 cm) and B is the magnetic field (= 1 T) [16,20].

CD spectra were recorded at 20 nm/min scan rate with a resolution of 1.0 nm, summing up 8 spectra to improve the signal-to-noise ratio. All experiments were carried out with protein solutions freshly prepared before use, containing 1.0 μM protein in 5 mM phosphate buffer plus 10 mM NaCl at pH 7.0 and titrated with HCl/NaOH.

2.5. Resonance Raman measurements

RR spectra were obtained at room temperature using the 404.8 nm line of a diode laser (MatchBox Series, Integrated Optics, Vilnius, Lithuania) and the 441.6 nm line of a He—Cd laser (Kimmon IK4121R-G, Tokyo, Japan). Backscattered light from a slowly rotating 5 mm NMR tube was collected and focused into a triple spectrometer (ActonResearch, Acton, MA), consisting of two SpectraPro 2300i instruments in subtractive mode, and a SpectraPro 2500i instrument in the final stage with a grating of 3600 grooves/mm (with a nominal resolution of 1.2 cm^{-1}) and equipped with a liquid N_2-cooled CCD detector (Roper Scientific Princeton Instruments).

The RR spectra wavenumbers were calibrated using indene and carbon tetrachloride as standards. The power on the sample was was 3.5 mW using the 441.6 excitation wavelength for the H64A ferrous sample, and 4 mW using the 404.8 excitation wavelength for all the ferric and ferrous samples, respectively. To improve the signal-to-noise ratio, the RR measurements were repeated several times and summed, only when no spectral differences were observed. The RR spectra were baseline-corrected and normalized in the high wavenumber region to the intensity of the ν_4 band, at 1360–1374 cm^{-1}, and in the low wavenumber region to the intensity of the ν_8 band, at 347–348 cm^{-1}. The intensity ratio of ν_4 to ν_8 was about 7.5 and 40 for the ferric and ferrous samples, respectively.

The total accumulation time and the number of the RR spectra are reported in **Table S1**.

A spectral deconvolution program (LabCalc; Galactic Industries, Salem, NH) was used to determine with an accuracy of 1 cm^{-1} the peak wavenumber, bandwidth, and intensity, assuming a Lorentzian line shape. In the figures, unless indicated, all the RR spectra are taken using the 404.8 nm excitation wavelength.

3. Results

3.1. hNgb-WT

A number of techniques have reported for murine Ngb, both in crystal and solution phases, the peculiar presence of the heme rotational disorder, where two heme conformers, resulting from the rotation by 180° about the α,γ-*meso* axis in the protein pocket, are found [6,21–27]. Unlike murine Ngb, in the crystal structure of wild-type hNgb no heme rotational disorder was detectable due to the lower resolution [5,6,25], but two independent monomers (namely, A and B), both hexacoordinated by the distal and proximal His64 and His96, respectively, forming a loosely assembled dimer, have been reported. The A and B monomers are not identical, differing considerably in the CD loop that contains Cys46 and Cys55. These two residues form a disulfide bridge, relevant for the binding of exogenous ligands, by decreasing the His64 binding affinity to the heme iron [19]. In addition, the two monomers remarkably differ also for the H-bonding interaction involving the two propionates of the heme macrocycle (see below). Evidence of two alternative heme orientations within the heme pocket has been provided in solution for the hNgb-WT by NMR [22,28].

Accordingly, in the RR solution spectra, as in murine Ngb [25,26], the ferric form of hNgb is characterized by a double set of core size marker bands (e.g. ν_3), arising from two hexacoordinated low-spin (6cLS) species, where the heme exists in two possible orientations [29]. As a consequence, due to the different conformations of the peripheral vinyl groups in the two conformers, four vinyl stretching modes (two for each heme) are expected. However, similarly to murine Ngb [25,26], at neutral pH the vinyl vibrations of the conformers overlap, and only two vinyl stretching bands were identified in the high wavenumber region, at 1620 and 1630 cm^{-1}, and three $\delta(C_\beta C_a C_b)$ bending modes at 400, 416, and 428 cm^{-1} in the low wavenumber region (Fig. 1) [29]. Based on the correlation between the torsional angles and the vinyl stretching wavenumbers [30] and by analogy with murine Ngb [26], we can conclude that the vinyl groups are in *cis* conformation for the reversed conformer (both $\nu_{C=C}$ stretching modes are at 1630 cm^{-1}, with corresponding $\delta(C_\beta C_a C_b)$ bending modes at 428 cm^{-1}), and in *cis/trans* conformations in the canonical conformer: $\nu_{C=C}$ stretching modes at 1630 and 1620 cm^{-1} for vinyls at positions 2 and 4 (v2 and v4), with corresponding $\delta(C_\beta C_a C_b)$ bending modes at 416 and 400 cm^{-1}, respectively (Fig. 1).

It has been already reported that between pH 3 and 12 several acid-base equilibria affect the electronic properties of ferric hNgb [16]. At extreme pH values, heme release from the protein matrix occur [12,31], while between pH 5 and 10 the acid-base equilibria have been suggested to involve the sidechains of non-coordinating aminoacids close to the heme and at least one heme propionate. In this pH range, the CD spectra of WT Ngb [12] showed little variation of helix content by changing pH. Similarly, the UV–Vis electronic absorption spectra hardly change as compared to the reported spectra at pH 7.4, being all characteristic of a 6cLS species in agreement with previous data [16]. Accordingly, the core size marker bands in the RR spectra are unaffected by the pH change from 3.7 to 12.3, indicating also no variation in the population of the two conformers due to the heme rotational disorder. However, it is worth noticing that, as increasing pH, in the RR spectra we observed differences on the vinyl stretching and bending modes only, while the propionate bending vibrations are not significantly affected (Fig. 1). In particular, the vinyl $\delta(C_\beta C_a C_b)$ bending mode intensity at 400 cm^{-1} does

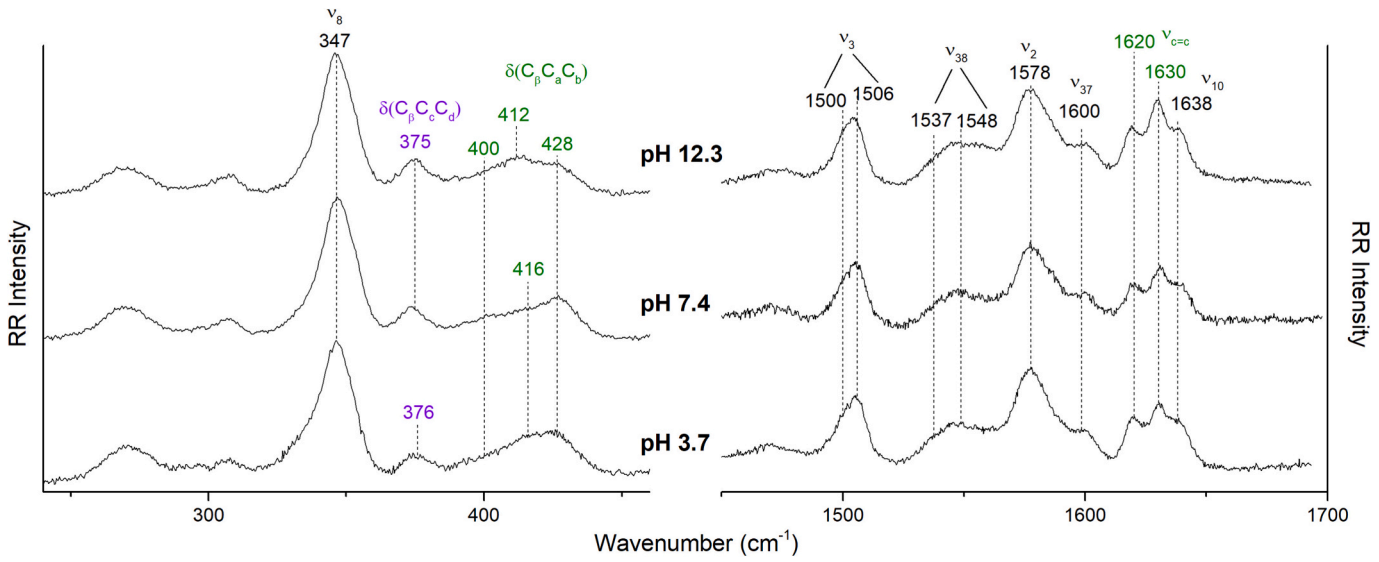

Fig. 1. RR spectra of the ferric hNgb-WT obtained at different pH values in the low (left) and high wavenumber regions (right). The 1450–1680 cm^{-1} region has been intensified by a factor 2 along the Y-axis. The propionate bending modes are reported in purple, while the vinyl bending and stretching vibrations are reported in green. (For interpretation of the references to colour in this figure legend, the reader is referred to the web version of this article.)

not change over the entire pH range, while the $\delta(C_\beta C_a C_b)$ bending mode at 428 cm^{-1} decreases in intensity as going from acid to alkaline pH. In addition, the band observed at 416 cm^{-1} at pH 3.7 and 7.4 appears to shift to 412 cm^{-1} at alkaline pH. In the high wavenumber region, the $\nu_{C=C}$ vinyl stretching modes show only a small change in their relative intensity, being the 1630 cm^{-1} vibration more intense at alkaline pH.

A better understanding of the contributions of the overlapped vibrations in the RR spectra has been obtained by a spectral deconvolution analysis (**Fig. S1**) which confirms the presence of two distinct ν_{10} bands in the 1600–1650 cm^{-1} region, assigned to the two heme conformers. Concomitantly, three $\nu_{C=C}$ vinyl stretching modes were also observed in the high wavenumber region at 1620, 1629, and 1631 cm^{-1} as for murine Ngb [26]. The intensity of the $\nu_{C=C}$ mode at 1629 cm^{-1} increases at the expense of that at 1631 cm^{-1}, as going from pH 3.7 to pH 12.3 (**Fig. S1**). However, the spectral deconvolution analysis reveals the presence of four $\delta(C_\beta C_a C_b)$ vinyl bending modes. Interestingly, the $\delta(C_\beta C_a C_b)$ vinyl bending modes in the low wavenumber region spectra show a similar pH-dependent trend with an increase of the band at 412 cm^{-1} at the expenses of that at 416 cm^{-1} at alkaline pH.

In the ferrous state at pH 7.4 hNgb-WT is a bis-histidyl 6cLS species as shown by the UV–Vis electronic absorption spectrum [32] and the RR core size marker bands (Fig. 2). In agreement with the ferric species, the vinyl substituents give rise to three $\delta(C_\beta C_a C_b)$ bending modes at 402, 413, and 429 cm^{-1} and two $\nu_{C=C}$ stretching modes at 1619 and 1630

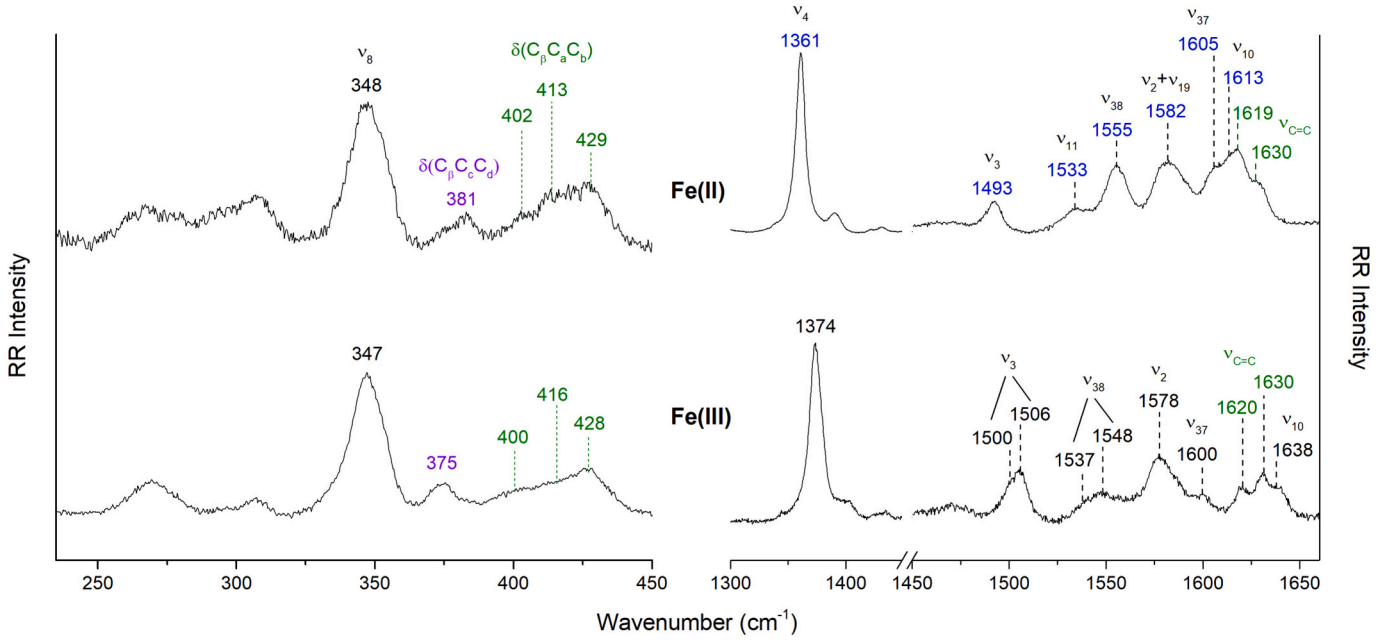

Fig. 2. RR spectra of ferric and ferrous hNgb-WT at pH 7.4 in the low (left) and high wavenumber regions (right). The 1450–1660 cm^{-1} region has been intensified by a factor 3 along the Y-axis. The core size marker bands of the Fe(III) 6cLS and Fe(II) 6cLS species are shown in black and blue, respectively. The propionate bending modes are reported in purple, while the vinyl bending and stretching vibrations are reported in green. (For interpretation of the references to colour in this figure legend, the reader is referred to the web version of this article.)

cm^{-1} (Fig. 2). These spectra are very similar to those observed for the ferrous murine Ngb [24] for which the presence of rotational disorder was suggested to explain the complex reactivity with ligands in the Fe (II) state [23]. Therefore, the rotational disorder is maintained in the ferrous form also for hNgb.

Between pH 5.2 and 11.4 no significant differences are observed in the high wavenumber region of the ferrous hNgb-WT. However, a spectral deconvolution analysis evidences a pH-dependent behavior: three $\nu_{C=C}$ stretching modes at 1619, 1625, and 1630 cm^{-1} are found and their relative intensities change upon pH increase, mainly resulting in the intensity decrease of the mode at 1625 cm^{-1} and a slight decrease of the mode at 1619 cm^{-1} at alkaline pH (**Fig. S2**). This effect is not as evident as for the ferric form in the RR spectra, possibly due to the overlap with the ν_{10} mode at 1613 cm^{-1}. On the contrary, as in the ferric state, in the low wavenumber region four vinyl bending vibrations at 402, 413, 421 and 429 cm^{-1} are shown by spectral deconvolution (**Fig. S2**). The analysis clearly indicates at alkaline pH the increase of the intensity of the $\delta(C_\beta C_a C_b)$ band at 413 cm^{-1} with the concomitant decrease of that at 429 cm^{-1}, similarly to the ferric hNgb-WT.

3.2. hNgb-H64A

Distal mutation alters the stability of the protein and the $pH_{1/2}$ of heme dissociation is around 4.5, about two units higher than the WT, and very similar to myoglobin [12]. However, as for the WT, the H64V [12] and the H64A variants (**Fig. S3**) also show very little helix content variation between pH 6 and 11. Mutation of the distal His64 alters the heme iron spin and coordination states as well. As observed for other hNgb-H64 mutants [13–15,33], the ferric hNgb-H64A variant at acidic pH is hexacoordinated high-spin (6cHS), being the distal His replaced by a water molecule. This is confirmed by the corresponding MCD and UV–Vis electronic absorption spectra (Fig. 3 and Fig. 4**, left**). The former is closely similar to those of proteins containing a 6cHS heme with a proximal His and a distal H_2O axial ligands [34–37], such as the imidazole adduct of the H93G mutant of sperm whale myoglobin [37], and features a derivative-shaped signal associated to the Soret band (peak, trough and cross-over point at 399, 416 and 408 nm, respectively) and three troughs in the visible region (at 543, 576 and 640 nm).

The RR spectrum at pH 6 (Fig. 4**, right**) is very similar to the one of myoglobin [38] and no rotational disorder has been observed. The only marked difference is the presence of two vinyl $\nu_{C=C}$ stretching modes at 1619 and 1630 cm^{-1} in the Ngb variant, while in Mb both stretching modes overlap at 1621 cm^{-1} [39]. Therefore, in H64A mutant, as in the WT protein, only one vinyl (characterized by the band at 1619 cm^{-1}) shows a maximum conjugation with the porphyrin macrocycle [30], explaining the overall blueshift of the UV–Vis spectrum by about 4–5 nm, as compared to Mb [40]. Accordingly, in the low wavenumber region two $\delta(C_\beta C_a C_b)$ vinyl bending modes at 409 and 419 cm^{-1} are observed (Fig. 5). Moreover, unlike the WT where the $\delta(C_\beta C_c C_d)$ propionate bending modes overlaps at 375 cm^{-1}, in the variant two bands are observed at 371 and 381 cm^{-1}. Changes in these vibrational modes indicate changes in H-bonding interactions with polar residues of the heme cavity [41]. Since an increase of the number and/or the strength of the H-bonds cause a shift to higher wavenumber, upon mutation one propionate increased the H-bond interaction.

Between pH 6 and 10 the protein undergoes a pH-induced transition toward a 6cLS species, ascribed to the coordination of the distal Ly67 to the Fe atom, in accordance with the results obtained for other Ngb-H64 mutants [13–15]. Indeed, upon increasing the pH from 6 to 10, both the MCD and UV–Vis spectra of H64A become (Figs. 3 and 4) closely similar to those of 6cLS heme proteins [34,36,37]. In particular, the S-shaped MCD signal associated with the Soret band red shifts (peak, trough and cross-over point at 402, 417 and 409 nm, respectively) and its peak-to-trough distance significantly increases, as expected for 6cLS hemes [42]. In addition, the trough at 640 nm, which is associated to the charge-transfer $a'_{2u}(\pi) \rightarrow e_g(d_\pi)$ band at 630 nm distinctive of ferric 5cHS and 6cHS heme proteins [43–45] (**Fig. 4**), disappears while a new derivative-shaped signal (peak, cross-over point and trough at 552, 559 and 573 nm) replaces the trough at 576 nm (Fig. 3), typical of 6cLS hemes [34,36,37,42]. Therefore, the pH-induced changes in the MCD spectra of hNgb-H64A fit with the progressive shift from a 6cHS form at pH 6 to 6cLS heme at alkaline pH values, in agreement with the replacement of the weak H_2O distal ligand with the much stronger amino N atom of Lys67. Upon further increasing the pH to 12, while no significant change in the wavelengths of the UV–Vis and MCD spectra of H64A occurs a decreased intensity of the latter is ascribed to pH-induced protein precipitation (Fig. 3), which does not affect the heme coordination, being the wavenumbers of the vibrations in the RR spectra the same between pH 10 and 12 (Fig. 4). The spin state transition at alkaline pH, observed also by the core size RR bands, is accompanied by change of the propionate and vinyl substituents vibrations (Fig. 4 **and** Fig. 5**).** The $\nu_{C=C}$ vinyl stretching mode at 1619 cm^{-1} is predominant at pH 6, while the $\nu_{C=C}$ mode at 1630 cm^{-1} becomes prevalent at alkaline pH. These data are confirmed by the spectral deconvolution in the 1600–1650 cm^{-1} region (**Fig. S4**).

In the low wavenumber region, the pH-induced transition causes changes of both the propionate and vinyl bending modes. In particular, the spectral deconvolution indicates that the two $\delta(C_\beta C_c C_d)$ propionate bending modes at 371 and 381 cm^{-1} at pH 6 shift to 367 and 375 cm^{-1} at alkaline pH, while the relative intensity of the $\delta(C_\beta C_a C_b)$ vinyl bending mode at 409 cm^{-1} strongly increases with respect to the other band at 419 cm^{-1} at alkaline pH, as compared to pH 6 (Fig. 5 **and Fig. S5**). Moreover, the weak band at 387 cm^{-1} is tentatively assigned to the stretching mode of the Fe(III)-N_{Lys67} bond, in analogy with the RR spectrum of the misligated His-Fe-Lys cytochrome *c* species [46], confirming the replacement of H_2O by Lys67 as the distal ligand of Fe(III) at

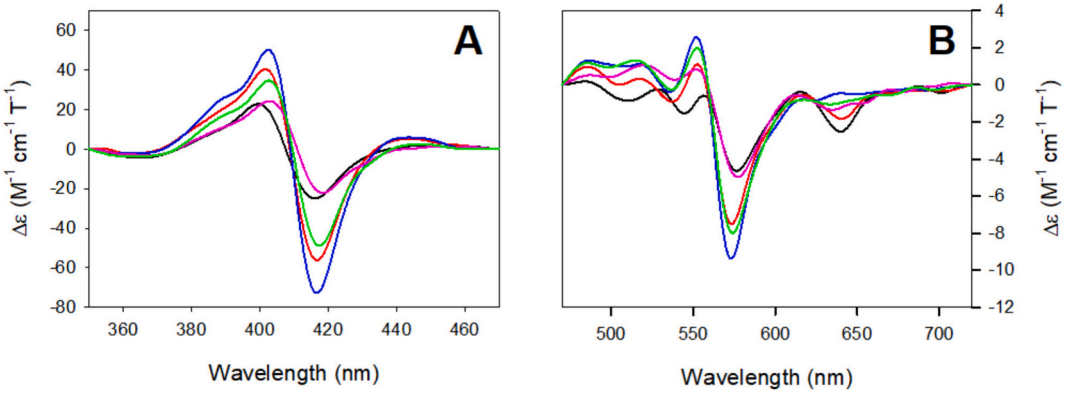

Fig. 3. MCD spectra of ferric hNgb-H64A in the Soret (left) and visible region (right) at different pH: pH 6 (black line), pH 7.5 (red line), pH 10 (blue line), pH 11.8 (green), and pH 12.1 (pink line). (For interpretation of the references to colour in this figure legend, the reader is referred to the web version of this article.)

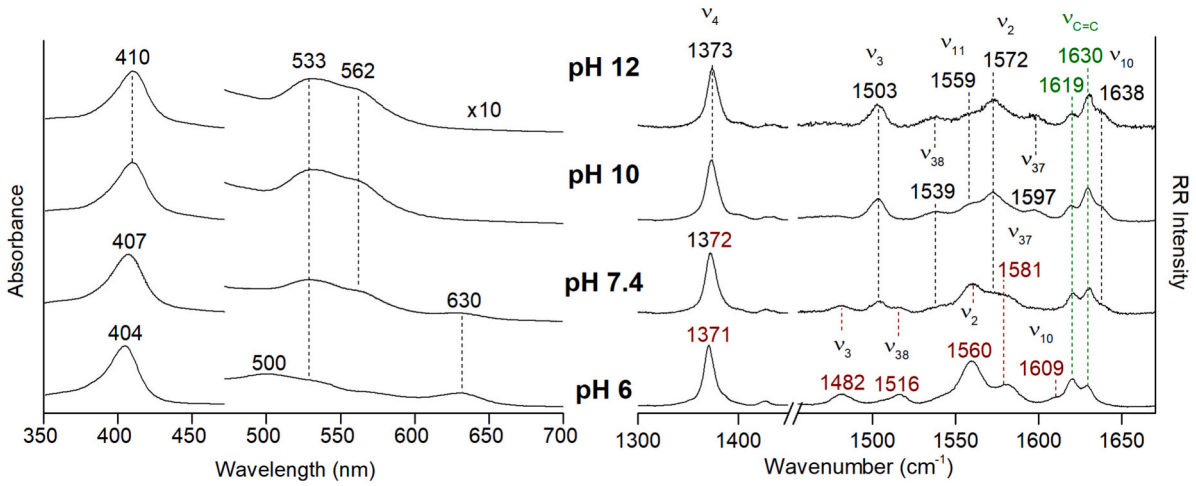

Fig. 4. UV–Vis and RR spectra of ferric hNgb-H64A at different pH values in the high wavenumber region. Left: the 470–700 nm region has been expanded 10 times. Right: the 1455–1670 cm^{-1} region has been intensified by a factor 2 along the Y-axis. The core size marker bands of the Fe(III) 6cLS and 6cHS species are shown in black and maroon, respectively. The vinyl stretching vibrations are reported in green. (For interpretation of the references to colour in this figure legend, the reader is referred to the web version of this article.)

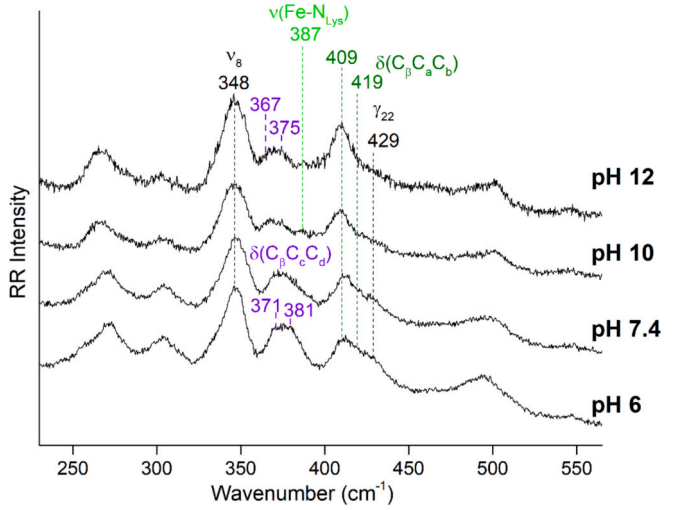

Fig. 5. RR spectra of ferric hNgb-H64A at different pH values in the low wavenumber region. The propionate bending modes are reported in purple, while the vinyl bending vibrations are reported in green. The ν(Fe-N_{Lys}) stretching mode is shown in light green. (For interpretation of the references to colour in this figure legend, the reader is referred to the web version of this article.)

alkaline pH values.

The Fe(II) protein at pH 6 is mainly a Fe-N_{His96} 5cHS species with a small amount of 6cLS, the latter becoming the only species at alkaline pH (Fig. 6). In the high wavenumber region of the RR spectra the overlapping contribution of the ν_{10} of the 6cLS species, expected around 1614 cm^{-1} [47], hampers to appreciate a relevant change of the intensity of the two vinyl stretching modes observed at 1618 and 1630 cm^{-1} at alkaline pH. However, from the spectral deconvolution (**Fig. S6**) it appears that, as in the ferric species, the band at 1630 cm^{-1} gains intensity at alkaline pH. Accordingly, in the low wavenumber region (Fig. 7), the vinyl bending modes are observed at 404 and 414 cm^{-1} at acid pH. As increasing the pH, the 414 cm^{-1} mode gains intensity at the expense of that at 404 cm^{-1}, while the propionate bending modes shift from 378 to 383 cm^{-1} at pH 9 (Fig. 7 **and S7**). Moreover, the comparison of the spectra at pH 6 obtained with two different excitation wavelengths (404.8 and 441.6 nm) allowed us to assign the ν(Fe-N_{His96}) stretching vibration at 220 cm^{-1}, which is intensified in resonance with the Soret band at 436 nm (Fig. 7**)** [48]. The wavenumber of this band is almost identical to that reported for the corresponding H64V variant [14].

4. Discussion

In neuroglobins, the distal His64 residue plays a crucial role in regulating ligand binding. Not only by controlling the accessibility of the heme iron to external ligands, acting as a gate for ligand entry, but also influencing the heme conformation. The p*K* of His64 in Ngb-WT is rather low due to the electrostatic interaction with the positive charge of Lys67, and His64 dissociation triggers a "heme sliding" movement, altering the heme position within the protein cavity [11,24,27,33,49]. In murine Ngb, due to the loose bonds necessary to allow heme sliding [6], the heme has been observed in both solution and crystal phases to exist in reversed and canonical orientations compared to the Mb structure, in a 70:30 proportion [21,24–26]. In solution, the RR spectra of hNgb are identical to those of murine Ngb [29], confirming the presence of rotational disorder, previously observed by NMR [22,28], with the reversed and canonical conformers in a similar ratio as in murine protein. The observed RR vinyl stretching (1620, 1629 and 1631 cm^{-1}) and vinyl bending modes (400, 412, 416, and 428 cm^{-1}) are due to the overlap of the vinyl group vibrations in *cis* and *trans* conformations, similarly to the murine Ngb-WT protein [25], indicating that the interactions between the vinyl and neighboring residues must be similar in the two proteins.

Although the overall secondary structure of both WT and H64V proteins has been reported to be unaffected in the investigated pH range [12], the present data clearly show that pH significantly alters the heme pocket and, in the absence of His64 residue, the reorganization of the distal cavity becomes significant.

In the WT, the stabilizing effect of the strong Fe-His64 bond prevents major changes of the heme coordination and spin states at alkaline pH, and, therefore, it does not affect the bis-histidyl hexacoordination. However, pH significantly alters the vinyl vibrations observed in both the ferric and ferrous forms. The changes in intensity of both the stretching and bending modes are consistent with a reorientation of a vinyl group, while the relative populations of the two conformers deriving from the heme rotational disorder do not vary in the whole investigated pH range (Fig. 8**)**. A similar relative intensity change of the vinyl bands has been previously observed in the CD loop-altered mutants of murine Ngb as compared to the WT. However, in that case, it was

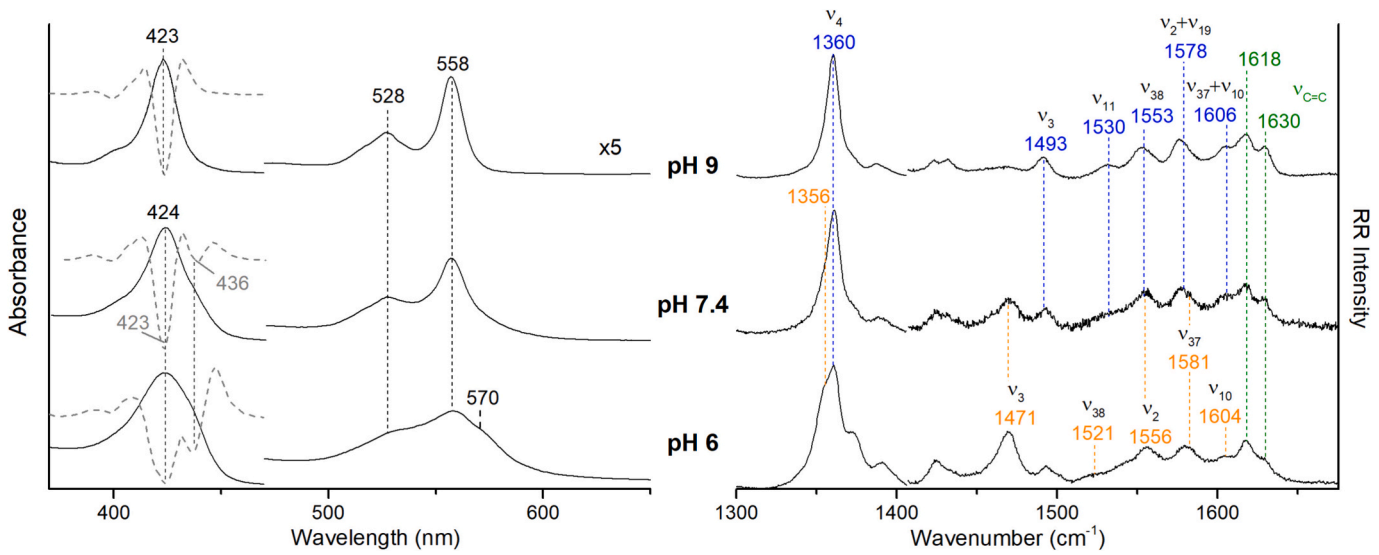

Fig. 6. UV–Vis and RR spectra of the ferrous hNgb-H64A at different pH values in the high wavenumber region. Left: the 470–700 nm region has been expanded 5 times. The second derivative spectra are reported in grey as dashed lines. Right: the 1405–1675 cm^{-1} region has been intensified by a factor 2 along the Y-axis. The core size marker bands of the Fe(II) 6cLS and 5cHS species are shown in blue and orange, respectively. The vinyl stretching vibrations are reported in green. (For interpretation of the references to colour in this figure legend, the reader is referred to the web version of this article.)

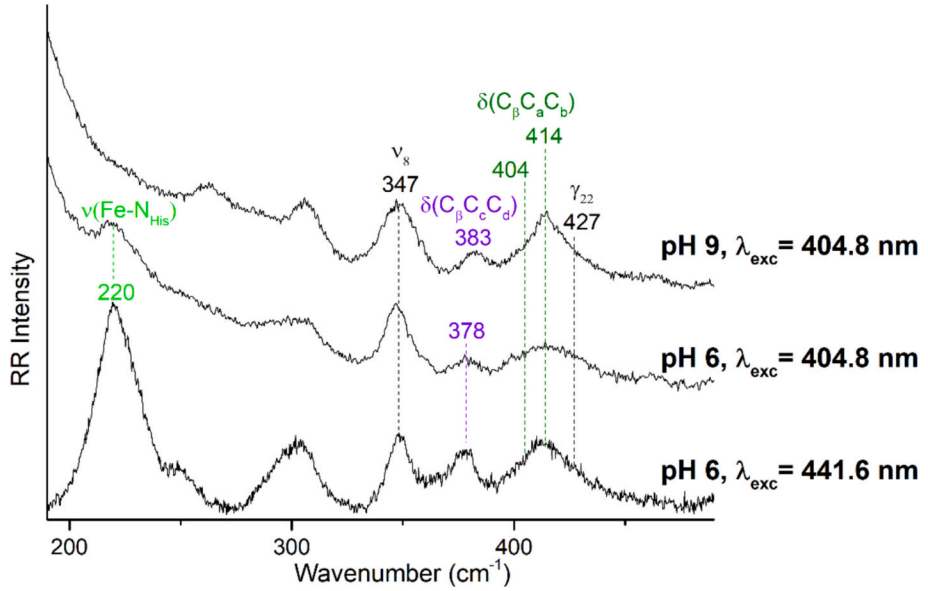

Fig. 7. RR spectra of ferrous hNgb-H64A variant at different pH values in the low wavenumber region at different excitation wavelengths (λ_{exc}). The propionate bending modes are reported in purple, while the vinyl bending vibrations are reported in green. The ν(Fe-N_{His}) stretching mode is shown in light green. (For interpretation of the references to colour in this figure legend, the reader is referred to the web version of this article.)

ascribed to a change in the population of canonical and reversed heme conformers since a concomitant change of the relative intensities of the core size marker bands of the two heme conformers was observed [25,27].

For WT hNgb, it has been suggested that the deprotonation of the ε-amino group of the solvent-exposed Lys67 can still occur at moderately alkaline pH values [16]. Therefore, it is reasonable to propose that the alkaline pH changes the protein electrostatic environment and the ionization state of amino acid residues, including Lys67. In fact, the Lys67 pKa is lowered below its usual value of 10.5, as a consequence of its role as a hydrogen bond donor in the complex array of H-bonds involving Tyr44, heme propionate at position 7 (p7), and water molecules within the heme pocket (Fig. 8). These changes result in a variation of the interactions between one vinyl with nearby residues in the heme pocket. Since Val68(E11) and Val71(E14) are within 4 Å from v4 in both A and B monomers of the crystal structure (Fig. 8), it is conceivable to suggest that a slight change in the *E*-helix due to the Lys67 deprotonation may alter the contact with this vinyl, changing its orientation. Residues in a 4 Å radius from v2 are located in the B, C and G-helices for both A and B monomers [5,7].

Conversely, the His64Ala mutation opens the distal cavity, giving rise at pH 6 to a 5cHS ferrous heme or to a 6cHS species in the ferric state, allowing the entrance of a water molecule, which binds the heme iron. The ferric hNgb-H64AK67A mutant displays identical UV–Vis and RR spectra to the H64A variant (data not shown), being an aquo 6cHS species at pH 6 as well. Therefore, the water molecule cannot be stabilized by Lys67, but probably by Glu60 as previously proposed [14], although in the WT structure [5] Glu60 is more than 13 Å far from the

	Monomer A			Monomer B		
	p6	p7	v4	p6	p7	v4
Tyr44					3.9 (O_2); 2.7 (O_2) - H_2O_{389} – 3.0	
Lys67 Nz		4.2 (O_1)			2.7 (O_1), 3.6 (O_2)	
H_2O_{328}				2.9 (O_2)	2.7 (O_1)	
H_2O_{394}	2.7 (O_2)	3.3 (O_1)				
Val68 O						4.1
CG1			4.2			3.9
Val 71 CG1			3.5			3.7
CB			3.8			3.8

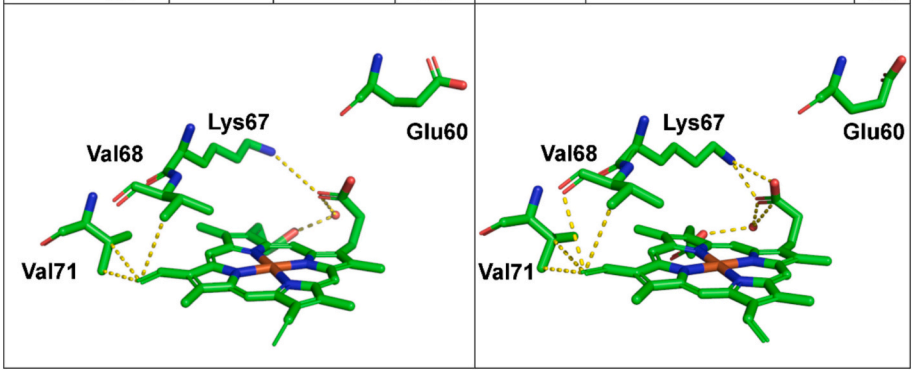

Fig. 8. Heme cavity structure of the hNgb-WT protein (PDB: 4MPM). In the A (left) and B (right) monomers, the yellow dashed lines indicate the interaction distances (within 4.2 Å, see table) between the Val71 and Val68 residues and the vinyl group at position 4 [5], the interactions between Lys67 and p7, and the water-mediated H-bond between the two propionates. The distal Glu60 residue is also depicted (see text). (For interpretation of the references to colour in this figure legend, the reader is referred to the web version of this article.)

heme iron, and a major distal reorganization should occur in this case.

Unlike the hNgb-WT, no evidence of rotational disorder has been found in the H64A variant, where only two vinyl stretching with the two corresponding bending modes have been observed. Moreover, in the variant the $\delta(C_\beta C_c C_d)$ propionate bending modes give rise to two bands observed at 371 and 381 cm^{-1} at pH 6, while in the WT the bending modes overlaps at 375 cm^{-1}. Since a shift to higher wavenumber indicates an increase of the strength of the hydrogen bonds, upon distal mutation one propionate forms a stronger H-bond as a consequence of the distal reorganization, which might involve the interaction with Lys67, being this residue H-bonded with both oxygens of p7 in the B monomer: p7(O_1)-N_{Lys67} distance is 2.7 Å and p7(O_2)-N_{Lys67} distance is 3.6 Å (Fig. 8) [5].

The alteration induced by alkaline pH causes further marked conformational changes allowing the entry of Lys67 into the cavity to bind the heme iron in both the heme Fe oxidation states of the protein. The change of the coordination and spin states from 6cHS to 6cLS is accompanied by a variation of both the propionate and vinyl substituents vibrational modes.

Clearly, the distal cavity is highly flexible since the ε-amino group of Lys67 should move into the cavity to bind the heme iron, being about 8 Å far from the metal atom in the native protein [5]. The rearrangement of the distal cavity brings about an alteration of both the heme peripheral substituents. The propionate bending vibrations are not affected by the pH in the WT protein since no major change in the pocket occurs, but in the H64A variant their wavenumbers shift in both the ferric and ferrous species. In the ferric state, the decreased wavenumber is consistent with the lowering of the strength of the H-bonds as a consequence of the loss of the interaction with Lys67 which binds to the Fe atom. However, the wavenumber increase observed in the ferrous form is more difficult to explain.

Furthermore, at alkaline pH marked changes in the relative intensities of both the vinyl streching and bending modes are observed, resulting from a change of the orientation of one vinyl group due to different steric hindrance exerted by the cavity. The mechanism might be similar to the WT, where a change of the contact between *E*-helix and vinyl at position 4 induces a change of its orientation. For the H64A variant, at alkaline pH a major readjustment of the E-helix can be envisaged following the binding of Lys67 to the heme iron.

5. Conclusions

The present data clearly show that alkaline pH significantly alters the heme pocket and in the absence of His64 residue the reorganization of the distal cavity becomes relevant, while the protein secondary structure is unaltered. We suggest that all changes are triggered by the deprotonation of Lys67. In the WT protein, the strong Fe-His64 bond prevents major rearrangement in the heme pocket, where only a vinyl substituent conformational change is observed. Conversely, the His64Ala mutation opens the cavity and the pH allows a major heme pocket conformational change with the entry and coordination of Lys67 to the heme iron, and a concomitant readjustment of the propionate H-bonds and orientation of the vinyl groups. These results, providing further molecular details on the influence of distal His64 and Lys67 residues on the heme pocket, support their pivotal role for heme complexation and stabilization within the protein cavity, and therefore for the regulation of exogenous ligand binding.

Declaration of competing interest

The authors declare that they have no known competing financial interests or personal relationships that could have appeared to influence the work reported in this paper.

Acknowledgments

This work was supported by the University of Modena and Reggio Emilia FAR Mission Oriented 2022 (Cobalt substituted globins as catalysts for electrochemical hydrogen production−G.B.) and by MUR-Italy ("Progetto Dipartimenti di Eccellenza 2023−2027", CUP

B97G22000740001 –DICUS 2.0, allocated to the Department of Chemistry "Ugo Schiff (F.S., G.S.).

Appendix A. Supplementary data

Supplementary data to this article can be found online at https://doi.org/10.1016/j.saa.2025.127401.

Data availability

Data will be made available on request.

References

[1] J. Tejero, C.E. Sparacino-Watkins, V. Ragireddy, S. Frizzell, M.T. Gladwin, Biochemistry 54 (2015) 722–733.
[2] S. Dewilde, L. Kiger, T. Burmester, T. Hankeln, V. Baudin-Creuza, T. Aerts, M. C. Marden, R. Caubergs, L. Moens, J. Biol. Chem. 276 (2001) 38949–38955.
[3] P. Ascenzi, A. di Masi, L. Leboffe, M. Fiocchetti, M.T. Nuzzo, M. Brunori, M. Marino, Mol. Aspects Med. 52 (2016) 1–48.
[4] C. Exertier, L.C. Montemiglio, I. Freda, E. Gugole, G. Parisi, C. Savino, B. Vallone, Mol. Aspects Med. 84 (2022) 101055.
[5] B.G. Guimaraes, D. Hamdane, C. Lechauve, M.C. Marden, B. Golinelli-Pimpaneau, Acta Crystallogr. D 70 (2014) 1005–1014.
[6] B. Vallone, K. Nienhaus, M. Brunori, G.U. Nienhaus, Proteins 56 (2004) 85–92.
[7] A. Pesce, S. Dewilde, M. Nardini, L. Moens, P. Ascenzi, T. Hankeln, T. Burmester, M. Bolognesi, Structure 11 (2003) 1087–1095.
[8] G. De Simone, D. Sbardella, F. Oddone, A. Pesce, M. Coletta, P. Ascenzi, Cells 10 (2021) 3366.
[9] M. Brunori, A. Giuffrè, K. Nienhaus, G.U. Nienhaus, F.M. Scandurra, B. Vallone, Proc. Natl. Acad. Sci. USA 102 (2005) 8483–8488.
[10] T. Brittain, Y. Yosaatmadja, K. Henty, IUBMB Life 60 (2008) 135–138.
[11] I. Birukou, R.L. Schweers, J.S. Olson, J. Biol. Chem. 285 (2010) 8840–8854.
[12] E. André, V. Derrien, P. Sebban, N. Assrir, E. Lescop, S. Bernad, J. Biol. Inorg. Chem. 24 (2019) 39–52.
[13] K. Nienhaus, J.M. Kriegl, G.U. Nienhaus, J. Biol. Chem. 279 (2004) 22944–22952.
[14] T. Uno, D. Ryu, H. Tsutsumi, Y. Tomisugi, Y. Ishikawa, A.J. Wilkinson, H. Sato, T. Hayashi, J. Biol. Chem. 279 (2004) 5886–5893.
[15] F. Trandafir, D. Hoogewijs, F. Altieri, P. Rivetti di Val Cervo, K. Ramser, S. Van Doorslaer, J.R. Vanfleteren, L. Moens, S. Dewilde, Gene 398 (2007) 103–113.
[16] M. Bellei, C.A. Bortolotti, G. Di Rocco, M. Borsari, L. Lancellotti, A. Ranieri, M. Sola, G. Battistuzzi, J. Inorg. Biochem. 178 (2018) 70–86.
[17] T. Burmester, B. Weich, S. Reinhardt, T. Hankeln, Nature 407 (2000) 520–523.
[18] D. Hamdane, L. Kiger, S. Dewilde, B.N. Green, A. Pesce, J. Uzan, T. Burmester, T. Hankeln, M. Bolognesi, L. Moens, M.C. Marden, Micron 35 (2004) 59–62.
[19] D. Hamdane, L. Kiger, S. Dewilde, B.N. Green, A. Pesce, J. Uzan, T. Burmester, T. Hankeln, M. Bolognesi, L. Moens, M.C. Marden, J. Biol. Chem. 278 (2003) 51713–51721.
[20] F. Paulat, N. Lehnert, Inorg. Chem. 47 (2008) 4963–4976.
[21] W. Du, R. Syvitski, S. Dewilde, L. Moens, G.N. La Mar, J. Am. Chem. Soc. 125 (2003) 8080–8081.
[22] J. Xu, L.Z. Li, G.W. Yin, H.L. Li, W.H. Du, J. Inorg. Biochem. 103 (2009) 1693–1701.
[23] A. Fago, A.J. Mathews, S. Dewilde, L. Moens, T. Brittain, J. Inorg. Biochem. 100 (2006) 1339–1343.
[24] C. Exertier, L. Milazzo, I. Freda, L.C. Montemiglio, A. Scaglione, G. Cerutti, G. Parisi, M. Anselmi, G. Smulevich, C. Savino, B. Vallone, Sci. Rep. 9 (2019) 5326.
[25] L. Milazzo, C. Exertier, M. Becucci, I. Freda, L.C. Montemiglio, C. Savino, B. Vallone, G. Smulevich, FEBS J. 287 (2020) 4082–4097.
[26] F. Sebastiani, L. Milazzo, C. Exertier, M. Becucci, G. Smulevich, J. Raman Spectrosc. 52 (2021) 2536–2549.
[27] C. Exertier, F. Sebastiani, I. Freda, E. Gugole, G. Cerutti, G. Parisi, L. C. Montemiglio, M. Becucci, C. Viappiani, S. Bruno, C. Savino, C. Zamparelli, M. Anselmi, S. Abbruzzetti, G. Smulevich, B. Vallone, ACS Chem. Biol. 17 (2022) 2099–2108.
[28] A. Bocahut, V. Derrien, S. Bernad, P. Sebban, S. Sacquin-Mora, E. Guittet, E. Lescop, J. Biol. Inorg. Chem. 18 (2013) 111–122.
[29] M. Meglioli, F. Sebastiani, M. Bellei, G. Di Rocco, A. Ranieri, C.A. Bortolotti, M. Sola, M. Borsari, G. Smulevich, G. Battistuzzi, Inorg. Chem. 64 (2025) 9066–9083.
[30] M.P. Marzocchi, G. Smulevich, J. Raman Spectrosc. 34 (2003) 725–736.
[31] P. Picotti, S. Dewilde, A. Fago, C. Hundahl, V. De Filippis, L. Moens, A. Fontana, FEBS J. 276 (2009) 7027–7039.
[32] D. Giordano, I. Boron, S. Abbruzzetti, W. Van Leuven, F.P. Nicoletti, F. Forti, S. Bruno, C.H. Cheng, L. Moens, G. di Prisco, A.D. Nadra, D. Estrin, G. Smulevich, S. Dewilde, C. Viappiani, C. Verde, PloS One 7 (2012) e44508.
[33] L. Astudillo, S. Bernad, V. Derrien, P. Sebban, J. Miksovska, Biochemistry 51 (2012) 9984–9994.
[34] L. Vickery, T. Nozawa, K. Sauer, J. Am. Chem. Soc. 98 (1976) 343–350.
[35] E. Droghetti, S. Sumithran, M. Sono, M. Antalik, M. Fedurco, J.H. Dawson, G. Smulevich, Arch. Biochem. Biophys. 489 (2009) 68–75.
[36] G. Battistuzzi, C.A. Bortolotti, M. Bellei, G. Di Rocco, J. Salewski, P. Hildebrandt, M. Sola, Biochemistry 51 (2012) 5967–5978.
[37] A.E. Pond, M.P. Roach, M.R. Thomas, S.G. Boxer, J.H. Dawson, Inorg. Chem. 39 (2000) 6061–6066.
[38] G. De Simone, A. di Masi, A. Pasquadibisceglie, A. Coletta, F. Sebastiani, G. Smulevich, M. Coletta, P. Ascenzi, J. Inorg. Biochem. 250 (2024) 112387.
[39] S.Z. Hu, K.M. Smith, T.G. Spiro, J. Am. Chem. Soc. 118 (1996) 12638–12646.
[40] G. De Sanctis, G. Petrella, C. Ciaccio, A. Feis, G. Smulevich, M. Coletta, Biophys. J. 93 (2007) 2135–2142.
[41] E.S. Peterson, J.M. Friedman, E.Y. Chien, S.G. Sligar, Biochemistry 37 (1998) 12301–12319.
[42] M.R. Cheesman, C. Greenwood, A.J. Thomson, Adv. Inorg. Chem. 36 (1991) 201–255.
[43] F. Neri, D. Kok, M.A. Miller, G. Smulevich, Biochemistry 36 (1997) 8947–8953.
[44] G. Smulevich, M. Paoli, G. DeSanctis, A.R. Mantini, F. Ascoli, M. Coletta, Biochemistry 36 (1997) 640–649.
[45] M.W. Makinen, A.K. Churg, in: A.B.P. Lever, H.B. Gray (Eds.), Iron Porphyrins, Addison-Wesley, London-Amsterdam, 1983, pp. 141–235.
[46] L. Milazzo, L. Tognaccini, B.D. Howes, G. Smulevich, J. Raman Spectrosc. 49 (2018) 1041–1055.
[47] S. Choi, T.G. Spiro, K.C. Langry, K.M. Smith, D.L. Budd, G.N. La Mar, J. Am. Chem. Soc. 104 (1982) 4345–4351.
[48] O. Bangcharoenpaurpong, K.T. Schomacker, P.M. Champion, J. Am. Chem. Soc. 106 (1984) 5688–5698.
[49] B. Vallone, K. Nienhaus, A. Matthes, M. Brunori, G.U. Nienhaus, Proc. Natl. Acad. Sci. USA 101 (2004) 17351–17356.